Published in final edited form as:
Neurobiol Aging. 2012 September ; 33(9): 2029–2045. doi:10.1016/j.neurobiolaging.2011.06.027.

Distinctive disruption patterns of white matter tracts in Alzheimer's disease with full diffusion tensor characterization

Hao Huang[1,2,*], **Xin Fan**[1], **Myron Weiner**[3,4,5], **Kristin Martin-Cook**[3,4], **Guanghua Xiao**[6], **Jeannie Davis**[1], **Michael Devous**[2,5], **Roger Rosenberg**[3,4], and **Ramon Diaz-Arrastia**[3,4,5]

[1]Advanced Imaging Research Center, University of Texas Southwestern Medical Center

[2]Department of Radiology, University of Texas Southwestern Medical Center

[3]Department of Psychiatry, University of Texas Southwestern Medical Center

[4]Department of Neurology, University of Texas Southwestern Medical Center

[5]Alzheimer's Disease Center, University of Texas Southwestern Medical Center

[6]Department of Clinical Sciences, University of Texas Southwestern Medical Center

Abstract

To characterize the white matter structural changes at the tract level and tract group level, comprehensive analysis with four metrics derived from DTI, fractional anisotropy (FA), mean diffusivity (MD), axial diffusivity (AxD) and radial diffusivity (RD), was conducted. Tract groups, namely limbic, commissural, association and projection tracts, include white matter tracts of similar functions. DTI data were acquired from 61 subjects (26 AD, 11 subjects with amnestic mild cognitive impairment or aMCI, 24 age-matched controls). An atlas-based approach was used to survey 30 major cerebral white matter tracts with the measurements of FA, MD, AxD and RD. Regional cortical atrophy and cognitive functions of AD patients were also measured to correlate with the structural changes of white matter. Synchronized structural changes of cingulum bundle and fornix, both of which are part of limbic tract group, were revealed. Widespread yet distinctive structural changes were found in limbic, commissural, association and projection tract groups between control and AD subjects. Specifically, FA, MD and RD of limbic tracts, FA, MD, AxD and RD of commissural tracts, MD, AxD and RD of association tracts and MD and AxD of projection tracts are significantly different between AD patients and control subjects. In contrast, the comparison between aMCI and control subjects shows disruption only in the limbic and commissural tract groups of aMCI subjects. MD values of all tract groups of AD patients are significantly correlated to cognitive functions. Difference between AD and control and that between MCI and control indicates a progression pattern of white matter disruption from limbic and commissural tract group to other tract groups. High correlation between FA, MD and RD measurements from limbic tracts and cortical atrophy suggests the disruption of the limbic tract group is caused by the neuronal damage.

*Corresponding Author: Advanced Imaging Research Center University of Texas Southwestern Medical Center 5323 Harry Hines Blvd, Dallas, TX 75390-8542 Tel: 214-645-2881 Fax: 214-645-2744 hao.huang@utsouthwestern.edu.

Disclosure Statement: There are no actual or potential conflicts of interest for any author.

Keywords

Alzheimer's disease; atlas; DTI; white matter tract; tract group; biomarker

Introduction

Alzheimer disease (AD) is a progressive brain disease of older adults. Early structural magnetic resonance imaging (MRI) detected hippocampal atrophy (e.g. Jack et al., 1999) and cortical thinning (Janke et al., 2001; Thompson et al., 2001; Thompson et al., 2003) in AD patients. In the metabolic imaging studies of gray matter, hypometabolism of the medial temporal lobe has been found with positron emission tomography (PET) (e.g. De Santi et al., 2001; Nestor et al., 2003). Although AD is generally considered to affect primarily gray matter, pathological evidence on white matter damages is also widespread (Scheltens et al., 1995; Smith et al., 2000, Gouw et al., 2008) and are believed to be related to axonal damage and breakdown of oligodendrocytes and myelin (Smith et al., 2000; Roher et al., 2002; Bartzokis, 2004; Bartzokis et al., 2007). Brain white matter is often categorized into different tract groups including limbic, commissural, association and projection tracts. The white matter tracts within a tract group perform similar functions. For example, limbic tracts underlie the connectivity in the limbic system and association tracts connect between cerebral cortical areas. Since cortical gray matter loss and brain function loss in AD patients are not uniform, we postulate that there are distinctive white matter disruption profiles which may demonstrate heterogeneous pathologic processes affecting different tract groups.

Diffusion tensor imaging (DTI), a modality of MRI that measures water diffusion properties noninvasively, is highly sensitive to subtle structural changes of white matter (Moseley et al., 1990; Basser et al. 1994). Although several metrics can be derived from diffusion tensor and these metrics characterize different aspects of diffusion tensors, fractional anisotropy (FA) (Pierpaoli et al., 1996; Beaulieu 2002) and mean diffusivity (MD), describing the shape and size of the diffusion tensor respectively, have been predominantly analyzed in AD. Two additional DTI-derived metrics, axial diffusivity (AxD) and radial diffusivity (RD), may provide more detailed information about the underlying pathology, as changes of AxD and RD are associated with the secondary degeneration of axons (Pierpaoli et al., 2001) and breakdown of myelin (Song et al., 2002; Song et al., 2003), respectively. These metrics have been studied in other neurological diseases such as multiple sclerosis (e.g. Henry et al., 2003; Roosendall et al., 2009) and very recently have received attention in AD (Acosta-Cabronero et al., 2010; Pievani et al, 2010).

Two major approaches have been mainly applied in AD to compare the values of DTI-derived metrics: regions of interest (ROI) (Stahl et al., 2007; Takahashi et al., 2002; Zhang et al., 2007, Mielke et al, 2009) and voxel-based morphometry (VBM) (Head et al., 2004; Xie et al., 2006, Medina et al, 2006; Damoiseaux et al, 2009, Acosta-Cabronero et al., 2010). The ROI approach can target specific regions of the brain and obtain measured parameters, but requires *a priori* information about brain regions likely to be affected. VBM compares the voxels of the entire brain in an unbiased fashion, but cannot characterize the changes at the tract level. Several recent studies on white matter disruption of AD focused on delineating the structural changes at the tract level (Stricker et al., 2009; Pievani et al., 2010). In this study, besides comprehensive survey at the tract level by covering almost all cerebral white matter, we extend the measurements of all DTI parameters at the tract group level. By transferring the white matter labeling from a digital white matter atlas (Mori et al., 2008) to DTI data of participating subjects in the common template space with nonlinear registration, the DTI-derived metrics of entire white matter tracts can be assessed, allowing inspection of the white matter structural changes at the tract level. By combining the

parameters of several white matter tracts belonging to the same tract group, the structural changes can be further characterized at the level of tract group.

DTI and T1-weighted images were acquired from 61 subjects (26 AD, 11 aMCI, 24 age-matched controls). 30 major cerebral white matter tracts were surveyed with a full tensor characterization including DTI-derived metrics FA, MD, AxD and RD. These 30 major tracts cover most of the limbic, commissural, association and projection white matter. After the white matter tracts were identified by transferring the labeling of digital white matter atlas (Mori et al, 2008), values at core white matter were used to alleviate the partial volume effects by adopting the skeletonization and projection steps of TBSS (Smith et al., 2006). The statistical differences of FA, MD, AxD and RD between AD and control were assessed at both the tract level and tract group level while differences between aMCI and control assessed at the tract group level. In addition, cortical atrophy and cognitive functions of AD patients were measured for correlation to all DTI measurements of the four tract groups. Specifically, cognitive functions were quantified with the CERAD test (Morris et al., 1989) for all subjects. Cortical atrophy of all cortical voxels was characterized with the RAVENS maps (Davatzikos et al., 2001) that reflect the regional tissue volumes in a normalized space with T1-weighted images.

Materials and Methods

Subjects and cognitive testing

A total of 61 subjects (26 AD, 11 aMCI and 24 age-matched normal subjects) were recruited for this study from longitudinally followed cohorts at the UT Southwestern Alzheimer's Disease Center, where neuropsychological assessment and disease staging are routinely performed according to the guidelines of the National Alzheimer's Coordinating Center Uniform Data Set (NACC UDS). All of the recruited subjects had some degree of white matter hyperintensities (WMH). None of the AD patients have vascular dementia based on standard NINDS-AIREN diagnostic criteria (Román et al., 1993), in that (1) they did not have a history of clinical stroke; (2) they did not have focal neurologic findings; (3) MRI did not show any cortically-based infarctions; (4) Hachinski score was < 4 (in most cases <2). Control subjects had no history of a psychiatric or neurological disease, and did not have a cognitive complaint. Additional criteria for control group were normal cognition and Clinical Dementia Rating (CDR; Morris 1993) score =0. Additional criteria for AD/aMCI group included a diagnosis of probable AD based on NINCDS/ADRDA criteria (McKhann et al., 1984) or a diagnosis of MCI based on Petersen criteria (Peterson et al., 1997), with CDR score=0.5-1. All subjects gave written informed consent prior to participation and the protocols of this study were approved by the institutional review board (IRB).

All subjects were administered the CERAD Neuropsychological Battery (Morris et al., 1989) by staff of the Alzheimer's Disease Center at UT Southwestern Medical Center at Dallas. The CERAD battery is a group of neuropsychological tests that assess attention, verbal fluency, memory, executive function and constructional praxis. A total score was derived by the method described from literature (Chandler et al., 2005) for each subject. Scores range from 0 to 100, with higher scores indicating better cognitive function.

Acquisition of DTI, FLAIR and T1-weighted image

A 3T Philips Achieva MR system was used. DTI data were acquired using a single-shot echo-planar imaging (EPI) sequence with SENSE parallel imaging scheme (SENSitivity Encoding, reduction factor =2.3). The imaging matrix was 112×112 with a field of view (FOV) of 224×224mm (nominal resolution of 2mm), which was zero filled to 256×256. Axial slices of 2.2mm thickness were acquired parallel to the anterior-posterior commissure

line (AC-PC). A total of 65 slices covered the entire hemisphere and brainstem without gap. The echo time (TE) and repetition time (TR) were 97ms and 7.78s without cardiac gating. The diffusion weighting was encoded along 30 independent orientations (Jones et al., 1999) and the b value was 1000s/mm^2. Imaging time for each sequence was 5 minutes and 15 seconds. To increase the signal-to-noise ratio (SNR), two repetitions were performed, with a total imaging time of 12 minutes. AIR (Woods et al., 1998) was performed on raw diffusion weighted images to correct distortion caused by eddy current. Six elements of the 3×3 diffusion tensor were determined by multivariate least-square fitting of diffusion weighted images. The tensor was diagonalized to obtain three eigenvalues (λ_{1-3}) and eigenvectors (ν_{1-3}). Anisotropy was measured by calculating FA (Pierpaoli and Basser, 1996). The tensor fitting was done using DtiStudio (Jiang et al., 2006). FA, MD, AxD and RD were determined by following equations of eigenvalues:

$$\begin{aligned} FA &= \frac{\sqrt{(\lambda_1-\lambda_2)^2+(\lambda_1-\lambda_3)^2+(\lambda_2-\lambda_3)^2}}{\sqrt{2}\sqrt{\lambda_1^2+\lambda_2^2+\lambda_3^2}} \\ MD &= (\lambda_1+\lambda_2+\lambda_3)/3 \\ AxD &= \lambda_1 \\ RD &= (\lambda_2+\lambda_3)/2 \end{aligned} \quad (1)$$

Fluid-Attenuated Inversion Recovery (FLAIR) MRI parameters were as follows, TR=11000ms, TI=2800ms, TE=125ms, in-plane FOV=224×224mm, in-plane dimension: 512×512, 24 slices with thickness 5mm and gap 1mm. Co-registered magnetization-prepared rapid gradient-echo (MPRAGE) images at resolution of 1×1×1mm were also acquired. MPRAGE images have superior gray and white matter contrast and were used for cortical segmentation and cortical atrophy calculation.

Atlas-based quantification at the tract level

This quantification integrated the digital white matter atlas and nonlinear registration, skeletonization and projection steps from TBSS. The digital white matter atlas was JHU ICBM-DTI-81 (http://cmrm.med.jhmi.edu/). TBSS was obtained from the website (FSL, http://www.fmrib.ox.ac.uk/fsl). JHU ICBM-DTI-81 is a probabilistic atlas generated by mapping DTI data of 81 subject to a template image. It has discrete labeling from 0 to 50. Fig. 1 demonstrates the process of atlas-based quantification. As shown in Fig. 1a, several TBSS functions were used to project the FA value of white matter to the skeleton or core of the white matter with FA data of all subjects at the atlas space. As described below, the single subject template used for nonlinear registration process in TBSS is identical to the template used for establishing the digital white matter atlas. We will call this template space ICBM-DTI-81 space hereafter. Fig. 1b is the ICBM-DTI-81 atlas. By transferring the labeling of the individual white matter tract, for example, genu of corpus callosum (GCC), we can label the skeleton FA data of all subjects in the ICBM-DTI-81 space, as shown in Fig. 1c. In this way, the atlas labeling is overlaid to the mean skeleton in the ICBM-DTI-81 space such that each skeleton voxel could be categorized into one of the major tracts. The details of the process are as follows:

1. To obtain the FA maps with cubic voxel size, the FA maps in the native subject space were sampled to the images with resolution 1.75×1.75×1.75mm^3 by trilinear interpolation.
2. FA maps of all subjects were then nonlinearly registered by TBSS to the so-called “EVE” template (http://cmrm.med.jhmi.edu/), which is the FA map serving as the template to generate the ICBM-DTI-81 atlas. The FA map of “EVE” template came from a single subject which has sharper contrast than the blurred average FA map. This FA map was also downsampled to the resolution 1.75×1.75×1.75mm^3 and

cropped to the same dimension as those of sampled subject FA maps from step #1. This step ensures that all our FA maps are well registered to the ICBM-DTI-81 atlas.

3. After nonlinear registration in step #2, the entire aligned dataset was transferred by affine transformation and zero padded into the ICBM-DTI-81 space which has the labeling of white matter structures and dimension of 182×218×182 with $1\times1\times1mm^3$ resolution. In the ICBM-DTI-81 space, a mean FA skeleton was created with skeletonization process of TBSS. Each subject's FA data was projected onto this skeleton with the TBSS projection process. FA data of all subjects were then projected to the core white matter skeleton in the ICBM-DTI-81 space and all skeleton voxels of core white matter had the labeling of white matter tracts transformed from the digital atlas of ICBM-DTI-81.

4. For non-FA images including MD, AxD and RD, the same nonlinear registration obtained in step #2 was applied to transform them to the ICMB-DTI-81 space and the same skeleton projection in step #3 was also used to get the MD, AxD and RD values at the skeleton voxels.

Cortical atrophy calculation

We investigated the gray matter volume changes in AD patients through the RAVENS maps (Davatzikos et al., 2001) that reflect the regional tissue volumes in a normalized space. The T1-weighted images (MPRAGE) of all subjects were skull-stripped by the FSL BET toolbox and were segmented into three tissue types as gray matter, white matter and ventricle by the HAMMER package from the SBIA of UPenn (https://www.rad.upenn.edu/sbia/). We then performed the nonlinear registration with the HAMMER algorithm (Shen and Davatzikos, 2002) to align the segmented tissue images to the Jacob fine-structure template provided in the HAMMER package. The RAVENS maps of cortical gray matter for all subjects in the Jacob template space were generated from the deformation fields given by the HAMMER registration process. After smoothing RAVENS maps with a Gaussian kernel (FWHM = 12mm) by SPM5 (http://www.fil.ion.ucl.ac.uk/spm/), we calculated Z-score maps [(patient individual value-controls mean)/standard deviation of controls] from RAVENS map to characterize the cortical atrophy. Regional cortical volumes were compared between AD and control with student t test and t values were obtained at each cortical voxel to illustrate the cortical atrophy patterns.

Mixed-effects statistics to compare DTI-derived metrics at the tract level

The multiple skeleton voxels of a specific white matter tract in the ICBM-DTI-81 space were considered as one group. Take FA value as an example. We used FA values of all skeleton voxels within each specific white matter tract to represent the integrity of this tract. The inter-subject comparison to detect disruption of individual white matter tracts was based on the group of FA values from all these skeleton voxels within this tract, rather than averaged FA value from these skeleton voxels. FA measurements at the skeleton voxels within the same tract are highly correlated and the following mixed-effects model was fitted for each tract to account for these correlations.

For FA value at any skeleton voxel in any major white matter tract of any participated subject, $FA_{i,j,k}$ was defined where i was the ith skeleton voxel of the tract, j denoted a specific tract and k denoted the participated control subject or AD patient. There were M tracts and N subjects, where M was 30 and N was 61. Hence j was from 1 to 30 and k was from 1 to 61. For any tract j, it consisted of S_j skeleton voxels and i was from 1 to S_j. FA measurement for skeleton voxel i at tract j of subject k can be constructed with the mixed-effects model as follows:

$$FA_{i,j,k}=\mu_j+\beta_j I_k+b_{j,k}+\varepsilon_{i,j,k} \quad (2)$$

Where μ_j was the overall mean of the FA measurements of tract j; I_k was the indicator variable with I_k=1 for AD or aMCI patient and I_k=0 for healthy control; β_j was the mean difference between FA measurements of AD or aMCI patients and controls at tract j; $b_{j,k}$ was the random variable to account for the correlation among skeleton voxels within tract j of any subject k; and $\varepsilon_{i,j,k}$ was error term. Both $b_{j,k}$ and $\varepsilon_{i,j,k}$ satisfied identical independent distribution (i.i.d) with standard deviation σ_b^2 and σ_e^2, respectively. The model was selected based on the Akaike Information Criterion (AIC) (Akaike 1974; Burnham and Anderson 1998).

The models were fitted using R NLME package (Pinheiro and Betes 2000). In order to specify an appropriate model, the data were explored using three-dimensional scatter plots and Trellis plots. The spatial correlation among voxels was explored using variogram (Banerjee 2004) and goodness of fit was checked by residual plots. The false discovery rate (FDR) was used to control the family-wise type-I error. A Beta-Uniform distribution (Pounds and Morris 2003) method was applied to calculate FDR by the R Group Comparison package (http://bioinformatics.mdanderson.org/Software/OOMPA/).

The above-mentioned procedures were repeated for non-FA images including MD, AxD and RD to make the tract level comparison of all these metrics. For validation purpose, comparisons of mean and median of the four DTI-derived metrics of each tract were also conducted with student t-test.

Mixed-effects statistics to compare DTI-derived metrics at the level of tract group and correlation with CERAD and cortical atrophy

The statistical model to compare DTI-derived metrics at the level of tract group was similar to what we used in the section above. The only difference was that the skeleton voxels of a tract group were extracted by combining the skeleton voxels of several white matter tracts categorized into this tract group. Again, FDR was used to control the family-wise type-I error. Boxplots were made by calculating the minimum, 25 percentile, median, 75 percentile and maximum values of DTI metrics of AD patients and control subjects. The multivariate regression analyses were used to correlate between the FA, MD, AxD or RD of the tract group and cognitive test scores (CERAD) and adjust for the factors of age and education with data from AD patients only. p-values less than 0.05 indicated statistically significant correlation. In addition, a linear regression model was applied to test if there is significant interaction effect of the diagnostic status of AD on the measurements of FA, MD, AxD and RD of all tract groups.

All DTI-derived metrics of all tract groups were correlated to Z-score at all cortical voxels. Z-scores represent cortical atrophy. Correlation coefficients and p values for correlation between DTI parameter of each tract group and cortical atrophy all over the cortical voxels were calculated. We fitted the p values with Beta-Uniform model (Pounds et al., 2003), from which we calculated the false discovery rate. In addition, Kolmogorov-Smirnov (K-S) tests were conducted to find out if there are significant differences of the correlations of the DTI parameters of limbic tract group to cortical atrophy, compared to those of other tract groups to cortical atrophy.

Results

Participants

Table 1 summarizes the demographics and clinical information for subjects whose DTI datasets underwent complete analysis described in the Materials and Methods section. There is no difference among the groups in age (p=0.44), gender (p=0.21), years of education (p=0.61) or Hachinski score (p=0.25). As expected, there is significant difference of MMSE (p<0.001) and CERAD (p<0.001) among the groups.

Parcellation of white matter tracts with the digital atlas

The ICBM-DTI-81 atlas assigns a unique label to each voxel in the ICBM-DTI-81 space to indicate that the voxel belongs to one of 30 well-documented deep white matter tracts. As shown in Fig. 2, the atlas labeling is overlaid on the white matter skeleton mask derived from the mean FA map in the ICBM-DTI-81 space. The underlying mean FA map is also shown. It is evident from all axial, coronal and sagittal sections that each core skeleton voxel is categorized into one of the 30 major tracts. As the template of nonlinear registration process in TBSS and that used for generating the ICBM-DTI-81 are the same, labeled white matter regions from the atlas match the mean FA map well and cover the entire core white matter skeleton, demonstrating the effectiveness and accuracy of our atlas-based process. Note that the peripheral skeleton voxels are not covered by the atlas labeling as the ICBM-DTI-81 atlas itself labels the white matter tracts from the probabilistic FA map of 81 normal subjects and the peripheral skeleton voxels have much inter-subject variability which makes the fixed labeling of these voxels impossible.

Difference of FA, MD, AxD and RD at tract level

FDR-corrected p values were calculated after mixed-effects statistical model to detect white matter abnormality at the tract level. The mean of AD, difference between the mean of AD and that of control, standard error of AD, t value, p value of FA, MD, AxD and RD were listed for each of the 30 cerebral tracts surveyed. The above-mentioned results of these tracts were categorized into limbic, commissural, association and projection tract groups, shown in Tables 2, 3, 4 and 5, respectively. Abbreviations of the tract names in these tables can be found in the legend of Fig. 2.

Most of fornix/stria terminalis (FX/ST-L, FX/ST-R), body of fornix (FX-B), cingulum bundle at cingulate gyrus (CGC-L, CGC-R) and cingulum bundle in the hippocampus (CGH-L, CGH-R) in limbic tract group have significantly lower FA, higher MD and higher RD, but no significant difference on AxD, as shown in Table 2. For commissural tracts in Table 3, genu, body and spelenium of corpus callosum (GCC, BCC and SCC) have higher MD, AxD and RD, but only BCC, which is the major component of the corpus callosum, has significantly smaller FA. The other two components of corpus callosum, GCC and SCC, show the trend of smaller FA in AD patients. Shown in Table 4, the superior longitudinal fasciculus (SLF-L, SLF-R), superior fronto-occipital fasciculus (SFO-L, SFO-R), and external capsule (EC-L, EC-R) generally have significantly higher MD, higher AxD and higher RD, but the changes of FA for most of these tracts are neither significant nor uniform. Specifically, the mean FA of SLF-R, SFO-R and EC-R of AD patients are even higher than those of control, while other association tracts show lower FA values. For project tracts in Table 5, a majority of anterior corona radiata (ACR-L, ACR-R), posterior corona radiate (PCR-L, PCR-R), superior corona radiate (SCR-L, SCR-R), anterior limb of internal capsule (ALIC-L, ALIC-R) and posterior limb of internal capsule (PLIC-L, PLIC-R) have significantly higher MD and AxD. The changes of FA and RD for most of the projection tracts are not significant or uniform for these two metrics. The comparisons using

mean and median of the DTI-derived metrics of the tracts listed in Tables 2 to 5 show consistently significant differences with slight variations of p values.

Synchronized FA, MD and RD changes of fornix (FX) and cingulum (CG), both of which are part of limbic tract group, are apparent with high correlation coefficients and small p values (<=0.0001 for all), as shown in Fig. 3. AxD measurements of FX and CG are not significantly changed from control to AD, as shown in Table 2. Concurrently, the correlation of AxD of FX and CG was found not significant either (not included in plots in Fig. 3).

Difference of FA, MD, AxD and RD at the level of tract group

Difference between AD and control—Viewed from full tensor characterization, the structural changes of white matter tract groups are distinctive from each other. The p values obtained by comparison of the DTI metrics of skeleton voxels within the tract group between AD and control are listed in Tables 2 to 5. The boxplots of Fig. 4 clearly illustrates the unique combinations on changes of FA, MD, AxD and RD for the four tract groups. Among them, commissural tract group features significant changes of all four DTI metrics while projection tract group shows significant changes of least (two) metrics. Both limbic and association tract groups have significant changes of three metrics, but these metrics are different for these two tract groups. The significant difference of widely used FA occurs only for limbic and commissural tract groups because RD increases either exceed increases of AxD for commissural tracts or there is no AxD increase for limbic tracts. On the contrary, no significant decrease of FA values were found for association and projection tract groups as AxD increases exceed increases of RD for association tracts or there is no RD increase for projection tracts. Increases of MD can be observed in all tract groups. Since MD is the linear summation of AxD and RD, significant increase of either AxD or RD causes higher MD.

The linear regression model revealed significant interaction effects of the status of AD on FA, MD and RD of limbic tract group, FA, MD, AxD and RD of commissural tract group, MD, AxD and RD of association tract group and MD and AxD of projection tract group. Fig. 5 uses the diagrams to demonstrate the significant interaction effects of AD on the DTI parameters.

Difference between aMCI and control—Table 6 displays the averaged measurements of aMCI tract groups, the difference of the measurements between aMCI and control and the p values. It is clear that in almost all cases the direction of the change from control to aMCI, namely the increase or decrease of certain DTI parameter, is aligned with the changes from control to AD (Tables 2 to 5). However, most of these changes are not as statistically significant as those in AD patients, suggesting that white matter disruption progresses from normal to aMCI and to AD. Only FA, MD and RD of limbic tract group and MD of commissural tract group are significantly different between aMCI and control.

Correlation between DTI metrics and CERAD scores and between DTI metrics and cortical atrophy

Only MD significantly correlates to CERAD with data of AD patients for all four tract groups and the correlation plots are shown in Fig. 6. Both AxD and RD are significantly correlated to two tract groups. Specifically, AxD is significantly correlated to commissural and association tract groups. And RD is significantly correlated to limbic and commissural tract groups. However, correlation between FA values and CERAD scores is significant for none of the tract groups.

The t-value map demonstrating the cortical atrophy pattern is shown in panel (a) of Fig. 7. FA and MD of all tract groups are significantly correlated to considerable amount of cortical voxels, even after FDR correction, indicating general correlation between FA and MD of all tract groups and cortical atrophy of entire cortex. The correlation coefficient maps for correlation between FA, MD, AxD and RD of limbic tract group and cortical atrophy are shown as panels (b) to (e) of Fig. 7. The correlation coefficients of FA, MD and RD of limbic tract group to cortical atrophy are generally much higher all over the cortex. The correlations of these parameters of limbic tract group are significantly different ($p<0.001$) from that of any other parameter of any other tract group with K-S tests, indicating that disruption of limbic tract group is more significantly correlated to cortical atrophy.

Discussion

Several major findings emerged with our investigation. First, heterogeneous disruption at the level of white matter tract group was revealed with full tensor (FA, MD, AxD and RD) characterization and comprehensive tract analysis. Second, the almost identical pattern of correlation coefficient maps between cortical atrophy and FA, MD and RD of limbic tract group and cortical atrophy map itself suggests the white matter disruption of limbic tract group is caused by cortical neuronal damage. Cortical atrophy has significant impact on white matter damage of other tract groups, but factors other than cortical atrophy may also play important roles. In addition, the structural changes of different tracts, characterized by DTI parameters, are synchronized within limbic tract group. This finding validates the tract group level strategy which characterizes the general structural changes pattern for white matter tracts performing similar brain functions. Finally, the MD values of all tract groups are significantly correlated to the cognitive functions, revealing a direct relationship between degeneration of cognitive functions and white matter abnormalities.

White matter structural changes in limbic and commissural tract groups

Disruption of limbic and commissural tracts in AD has been most widely reported. The tracts in these white matter systems showed significantly lower FA values (Figs 4 and 5; Tables 2 and 3), consistent with the literature (e.g. Takahashi et al., 2002; Xie et al., 2006; Stahl et al., 2007; Zhang et al., 2007). Degeneration of the limbic system is closely associated with AD. In the limbic system network, atrophy of hippocampal and parahippocampal regions (Stoub et al., 2006) and medial temporal lobe (Thompson et al., 2003) are well documented. Reduced white matter volume in the cingulum (Villain et al., 2008) has also been reported. The microstructural changes of the limbic tracts including FX and CG were detected in our study, with significantly lower FA and higher RD. These changes are likely related to demyelination and axonal loss (Song et al., 2002; Song et al., 2003) and causally related to cortical atrophy (Fig. 7). They also result in disconnection of the brain regions in the limbic system.

All four parameters show significant differences for the commissural tract group, indicated by Figs. 4-5 and Table 3. Among individual commissural tracts, only the BCC shows significantly lower FA, while GCC and SCC demonstrate a trend of FA decrease. As BCC takes a large portion of the entire CC, the commissural tract group follows the same tensor change profile as that of BCC. Commissural tracts in general connect the homologous cortical areas of two hemispheres. Besides cortical areas, the rostral inferior part of BCC connects subcortical nuclei and the caudal inferior part of BCC connects medial temporal lobe (Huang et al., 2005). This may explain the excessive RD increase of BCC compared to AxD and resultant FA decrease (Table 3) which is closer to the tensor change profile of the limbic tracts. However, the tensor change profile of GCC and SCC are different from BCC. Rather, they are identical to the profile of the association tract group (Tables 3 and 4). The functions of GCC and SCC are quite similar to those of association tracts, namely

connecting two cerebral cortical regions. GCC and SCC connect homologous cortical areas of two hemispheres while association tracts connecting the cortical areas of the same hemisphere. The identical tensor change profiles of GCC, SCC and association tracts are likely due to their involvement in the same networks connecting between and within frontal and occipital areas. Several ROI-based studies (e.g. Zhang et al., 2007, Milke et al., 2009) show significantly lower FA at SCC while there is no significance of FA at SCC in our measurements. This discrepancy may be due to the fact that different voxels were measured for SCC. Our SCC is a 3D structure and defined for the tract connecting two occipital lobes (Wakana et al, 2007; Mori et al, 2008). Previous studies (e.g. Zhang et al., 2007, Milke et al., 2009) used 2D manually delineated ROIs. Alternatively, as the sample size in each of these studies is modest, a large number of subjects may be needed to settle this issue.

White matter structural change of association and projection tract groups

Our results on association tracts (Table 4, Fig. 4) also support recent findings on association tracts from another group (Pievani et al., 2010). Unlike other tract groups, white matter abnormalities on projection tracts have been rarely reported. This is likely due to the fact that little pathology affecting the gray matter structures connected by projection tracts has been reported in AD. For example, projection tracts are mainly involved in the motor functions and these remain relatively intact in early and modest AD, and there is little evidence of neuronal loss in motor cortex. The projection tract group has the least two abnormal diffusion metrics (Figs. 4 and 5 and Table 5) compared to all other three tract groups. The tensor change profile of projection tract group is closest to that of the association tracts. The only difference between the projection tract group and association tract group is that myelin loss and axon diameter change that are apparent causes of increased RD in association tracts do not happen in projection tracts. It is plausible to attribute the increase of MD and AxD of projection tracts to the factors other than AD, such as white matter lesion or vascular pathology. However, MD of projection tract group is significantly correlated to CERAD (Fig. 6), suggesting the increases of MD are directly related to AD. Decreased tissue density was found in AD (Bronge et al 2002; Englund et al 1998) while underlying structures is maintained. In addition, qualitatively comparison of locations of the projection tracts and those of WMH revealed from FLAIR MRI indicates that a majority of them cluster around the ventricles. These two factors may explain partly the increase of MD and AxD of the projection tract group and some abnormalities of individual tracts in this tract group (Table 5). It should be noted that corticospinal tract (CST) was not included in the project tract group because transferring the CST labeling from the atlas to the subject data was prone to the registration error due to relatively small tract bundle size for CST.

Characteristic white matter disruption for different tract groups in AD and possible mechanism

Combined with the findings on limbic, commissural and association tracts, white matter in almost the entire brain was affected by AD. These structural alterations are heterogeneous and the interactions of AD on these tract groups differ from one tract group to another (Figs. 4 and 5). To understand these white matter structural changes, two questions appear to be important. First is how the white matter change of different tract groups are related to cortical atrophy, which has been well documented for AD patients (e.g. Janke et al., 2001; Thompson et al., 2001 and Thompson et al., 2003). Second is how these white matter disruption patterns progress from the early phase of illness (aMCI) to the advanced stage of AD.

For the relationship between white matter changes of different tract groups and cortical atrophy, we found that FA and MD of all tract groups are significantly correlated to

considerable amount of cortical voxels even after FDR correction, resulting in the significant correlation to the overall cortical atrophy. Moreover, FA, MD and RD of limbic tract group are more significantly correlated to cortical atrophy than any other parameter of any other tract. As illustrated in Fig. 7b, 7d and 7e, the patterns of correlation coefficient maps for FA, MD and RD and cortical atrophy are almost identical to the cortical atrophy map itself shown in Fig. 7a. In general, axonal damage can be initiated either by the degeneration of the cell bodies associated with these axons, or direct white matter injury. In the former case, structural disruptions in white matter tracts identified from DTI metrics is a consequence of cortical degeneration. Our findings suggest that this former mechanism takes place in AD. White matter disruption of limbic tract group is caused by the neuronal loss in the cortex and structural change of other tract groups are also significantly affected by cortical atrophy. Moreover, the characteristic profiles of diffusion tensor change of the four tract groups seem to follow the degeneration of the cortical areas to which these tracts connect. However, the mechanism for the influence of cortical neuronal loss on the commissural, association and projection tract groups is complicated and might be mixed with other factors such as decreased tissue density, destruction of intracellular compartments or glial alterations. In addition, the close similarity of the patterns of correlation coefficient maps (especially for MD and RD) to cortical atrophy map (Fig. 7) suggests that MD and RD of limbic tracts can serve as an alternative measure of cortical atrophy. The former metrics have the advantage of being directly measured from DTI while the latter usually needs a more complicated normalization process and additional control data. It is plausible to contribute the close resemblance of coefficient and cortical atrophy maps to misregistration due to cortical loss. This situation is not likely because of the validation of the registration discussed below and poor correlation of AxD in Fig. 7d.

From early phase to advanced stage of AD, Tables 2 to 6 imply that there is a pattern of white matter disruption which progresses along with disease evolution. Specifically, the white matter disruption takes place only in limbic and commissural tracts in aMCI subjects (Table 6) and progress to all four tract groups in AD patients (Tables 2 to 5). On the other hand, the degree of damage to white matter tracts affected in AD patients only (Tables 2 to 5) follows the gradient of most to least severe from limbic and commissural tracts to association and projection tracts. It suggests that the white matter tracts (i.e. limbic and commissural) suffering damages earlier in the aMCI phase will be more severely disrupted in the advanced stage of AD than those (i.e. association and projection) with no significant structural changes in aMCI phase. The heterogeneous damage of different white matter tract groups at early aMCI phase may underlie the distinctive structural changes in AD. Besides the aMCI results from this study, other investigations on aMCI (Huang et al., 2007; Zhang et al., 2007, Zhuang et al., 2010) also reveal white matter disruption mostly at limbic or commissural tracts. As this study is focused on the white matter damage of AD patients, the number of participated aMCI subjects is limited. A longitudinal study on the white matter tract groups from aMCI to severe AD from the same group of subjects will be needed to further test this hypothesis. Combining the discussion above on relationship between white matter damage, cortical atrophy and progression of white matter disruption from aMCI to AD, the progression of white matter disruption seems to follow the cortical thinning pattern spreading over time from temporal and limbic cortices into frontal and occipital cortices.

Features of analysis at tract level, tract group level and full tensor characterization

The development of a digital white matter atlas enabled us to automatically survey 30 major cerebral white matter tracts covering most of the limbic, commissural, association and projection tract groups. Conventional voxel-based approaches reveal abnormalities of white matter at the voxel level. Tract labeling provided by the digital atlas segments all the white matter and divides the white matter voxels into different tracts. In addition, white matter

tracts with similar functions can be combined together to form tract groups. Our study has presented the comprehensive white matter analysis at the level of tract groups.

Numerous findings on white matter disruption of AD have been reported, and controversy exists in the literature. Pathology based on postmortem brain tissues (e.g. Fazekas et al., 1993; Scheltens et al., 1995; Gouw et al., 2008) provides evidence of multiple mechanisms underlying the white matter damage, including loss of myelin, loss of oligodendrocytes, loss of axons, destruction of neurofibrils, and glial alterations. However, it is difficult to study the entire brain histopathologically, and microstructures are different *ex vivo* from *in vivo* due to fixation artifacts or morphological change of cells after death. Many previous DTI studies on AD focused on only part of the white matter, or used only some of the tensor metrics. Therefore, reports from these studies do not provide a complete picture on how white matter integrity changes are affected by AD. Thorough coverage of major cerebral white matter tracts with full tensor characterization may settle some of the controversial findings in the literature, and help to better characterize white matter damage *in vivo*.

Acosta-Cabronero et al. (Acosta-Cabronero et al., 2010) has recently pointed out that the white matter degeneration of AD needs full tensor information and that conventional interpretation based on FA alone has important limitations. Our findings support this opinion. Only with the full tensor characterization, the distinct tensor profile changes can be revealed, as shown in Fig. 4. Among the four tensor derived metrics, MD is the only one which is significantly correlated to the cognitive functions. It suggests MD is more sensitive than the other three metrics to the cognitive changes of AD. It is noteworthy that increased MD comes from different sources for different tract groups. For example, the higher MD in limbic tracts is mainly contributed by increase of RD while higher MD in project tracts is caused by the elevated AxD (Fig. 4). In addition, caution needs to be taken when interpreting the results of AxD and RD at crossing fiber areas (Wheeler-Kingshott and Cercignani 2009).

Technical considerations

In our exploratory data analyses, the DTI measurements of two voxels within the same tract are highly correlated, which motivated us to apply a mixed-effects model to account for the correlation. The distinguishing feature of mixed-effects model from other conventional measures is that it uses measurements of all voxels within the tract rather than just mean or median values of these measurements. We compared the results of mixed-effects model with those from conventional measures of median and mean values which are widely used. In terms of finding significant group differences in our study, the results from these three models are highly consistent with discrepancy in only less than 10% of all tracts. Because measurements of all voxels within the tract were used, the variance of β_j in equation (2) can be more accurately estimated in mixed-effects model. The differences of the estimation of variance of β_j from those obtained with conventional models could result in either oversensitive or less sensitive detection when this model is used to find the metric differences of two groups. The application of mixed-effects model to biomedical datasets with complex correlation structure is still under development. Until now, the most commonly used covariance structures have been compound symmetry and auto-regression model and there is no established statistical method that can incorporate the 3D spatial closeness between two voxels in DTI studies. In this study, we applied a mixed-effects model by assuming compound symmetry correlation structure, which is not sophisticated enough to take the 3D spatial closeness into account, although modeling a large proportion of the correlation among voxels within the same tract. With the advancement of the statistical methodology, it is likely that the statistical model including the factor of the spatial closeness will be established and these kinds of models will have great potential to the DTI analyses.

The anatomical definition of white matter tracts stems from the digital atlas (Mori et al, 2008). Like voxel-based analysis, this atlas-based approach greatly depends on the quality of nonlinear registration to transfer the atlas labeling to DTI data of individual subjects. To examine the validity of this approach, with the reverse transformation function provided by TBSS, the labeled skeleton voxels in the ICBM-DTI-81 space was projected back into the individual native subject space where DTI-based tractography was used to trace the major white matter tracts. The tractography (Mori et al., 1999) was applied to segment the deep white matter in the native subject space. Despite the underestimation caused by false negative results at the areas of crossing fibers, the validation indicated that all limbic tracts and callosal tracts and a majority of association and projection tracts had good matching (above or close to 90%) with the labeled skeleton voxels reversely transformed back to the native subject space. Inferior fronto-occipital fasciculi in both sides had especially low matching percentage, around 70%. There is still a controversy on the anatomy of this tract (Schmahmann and Pandya, 2006). And tractography shows that part of IFO and part of uncinate fasciculus (UNC) in their binary volume format overlap with each other in the frontal lobe. Hence the results of IFO and UNC are not included in Table 4. Several recently developed registration methods (e.g. Zhang et al., 2007, Chiang et al., 2008, Yap et al., 2009) have shown excellent quality especially for nonlinear registration of DTI data. They could be potentially incorporated to the atlas-based approach to nonlinearly transform the voxels of entire tracts from the subject space to template space. Other important factors which may influence the results are resolution and SNR of DTI data. Our DTI data has 2×2×2.2mm resolution, which is relatively higher than resolutions used in many clinical data (around cubic 2.5 to 3 mm). In addition, with two repetitions of data acquisition and usage of Jones 30 gradient (Jones et al., 1999) and a 3 T MR scanner, we tried to acquire the data with sufficient SNR. Many AD studies including a recent TBSS application (Damoiseaux et al., 2009) could not reveal as much white matter disruption as we have found in this study. It is tempting to contribute these differences to the factors of resolution and SNR. For example, Damoiseaux imaging protocol (Damoiseaux et al., 2009) indicates their DTI was acquired from 1.5 T MR scanner with one repetition and this DTI imaging protocol would cause relatively lower SNR. On the contrary, the widespread pattern of white matter damages with the parameters of MD, AxD and RD was also well observed by Acosta-Cabronero et al who used DTI data of quite high resolution and SNR, similar to those in our study.

Conclusions

A complete survey at the white matter tract level and tract group level revealed widespread and heterogeneous structural damage of white matter for AD patients. Full tensor characterization indicated tensor profile changes are distinctive among the four tract groups. Limbic and commissural tracts are characterized by the tensor changes which indicate demyelination and axonal loss while white matter structural changes of association and projection tracts may be more related to decreased tissue density. The almost identical pattern of correlation coefficient maps between cortical atrophy and FA, MD and RD of limbic tract group and cortical atrophy map itself suggests the white matter disruption of limbic tract group is caused by cortical neuronal damage. Difference between AD and control and that between MCI and control indicates a progression pattern of white matter disruption from limbic and commissural tract group to other tract groups. The significant correlation between MD values of all tract groups and the cognitive functions revealed the direct relationship of degeneration of cognitive functions and white matter abnormality.

Acknowledgments

This study is sponsored by NIH EB009545, NIH/NIA P30AG12300, NIH/NIA AG033106 and NIH 5UL1RR024982-02. The authors also thank The Alzheimer's Disease Center for recruiting AD patients and control subjects.

References

Acosta-Cabronero J, Williams GB, Pengas G, Nestor PJ. Absolute diffusivities define the landscape of white matter degeneration in Alzheimer's disease. Brain. 2010; 133:529–539. [PubMed: 19914928]

Alexander AL, Hasan KM, Lazar M, Tsuruda JS, Parker DL. Analysis of partial volume effects in diffusion-tensor MRI. Magn. Reson. Med. 2001; 45:770–780. [PubMed: 11323803]

Akaike H. A new look at the statistical model identification. IEEE Transactions on Automatic Control. 1974; 19:716–723.

Ashburner J, Friston KJ. Voxel-Based Morphometry--The Methods. NeuroImage. 2000; 11:805–821. [PubMed: 10860804]

Ashburner J, Friston KJ. Why Voxel-Based Morphometry Should Be Used. NeuroImage. 2001; 14:1238–1243. [PubMed: 11707080]

Banerjee, S. Hierarchical Modeling and Analysis for Spatial Data (Monographs on Statistics and Applied Probability). Chapman & Hall/CRC; 2004.

Bartzokis G. Age-related myelin breakdown: a developmental model of cognitive decline and Alzheimer's disease. Neurobiol. Aging. 2004; 25:5–18. [PubMed: 14675724]

Bartzokis G, Lu PH, Mintz J. Human brain myelination and amyloid beta deposition in Alzheimer's disease. Alzheimers Dement. 2007; 3:122–125. [PubMed: 18596894]

Basser PJ, Mattiello J, LeBihan D. MR diffusion tensor spectroscopy and imaging. Biophys. J. 1994; 66:259–267. [PubMed: 8130344]

Beaulieu C. The basis of anisotropic water diffusion in the nervous system-a technical review. NMR Biomed. 2002; 15:435–455. [PubMed: 12489094]

Benjamini Y, Hochberg Y. Controlling the false discovery rate: a practical and powerful approach to multiple testing. Journal of the Royal Statistical Society, Series B (Methodological). 1995; 57:289–300.

Bronge L, Bogdanovic N, Wahlund LO. Postmortem MRI and histopathology of white matter changes in Alzheimer brains. A quantitative, comparative study. Dement. Geriatr. Cogn. Disord. 2002; 13:205–212. [PubMed: 12006730]

Burnham, KP.; Anderson, DR. Model Selection and Inference - A practical information-theoretic approach. Springer-Verlag; 1998.

Chaim TM, Duran FL, Uchida RR, Perico CA, de Castro CC, Busatto GF. Volumetric reduction of the corpus callosum in Alzheimer's disease in vivo as assessed with voxel-based morphometry. Psychiatry Res. 2007; 154:59–68. [PubMed: 17174533]

Chandler MJ, Lacritz LH, Hynan LS, Barnard HD, Allen G, Deschner M, Weiner MF, Cullum CM. A total score for the CERAD neuropsychological battery. Neurology. 2005; 65:102–106. [PubMed: 16009893]

Chetelat G, Desgranges B, Landeau B, Mezenge F, Poline JB, Sayette, de la V, Viader F, Eustache F, Baron J-C. Direct voxel-based comparison between grey matter hypometabolism and atrophy in Alzheimer's disease. Brain. 2008; 131:60–71. [PubMed: 18063588]

Chiang MC, Klunder AD, Dutton RA, Barysheva M, Rose SE, McMahon KL, de Zubicaray GI, Toga AW, Thompson PM. Fluid registration of diffusion tensor images using information theory. IEEE Trans. Med. Imag. 2008; 27:442–456.

Damoiseaux JS, Smith SM, Witter MP, Sanz-Arigita EJ, Barkhof F, Scheltens P, Stam CJ, Zarei M, Rombouts SRRB. White matter tract integrity in aging and Alzheimer's disease. Hum. Brain Mapp. 2009; 30:1051–1059. [PubMed: 18412132]

Davatzikos C, Genc A, Xu D, Resnick SM. Voxel-based morphometry using the RAVENS maps: methods and validation using simulated longitudinal atrophy. NeuroImage. 2001; 14:1361–1369. [PubMed: 11707092]

De Santi S, de Leon MJ, Rusinek H, Convit A, Tarshish CY, Roche A, Tsui WH, Kandil E, Boppana M, Daisley K, Wang GJ, Schlyer D, Fowler J. Hippocampal formation glucose metabolism and volume losses in MCI and AD. Neurobiol. Aging. 2001; 21:19–26. [PubMed: 10794844]

Englund E. Neuropathology of white matter changes in Alzheimer's disease and vascular dementia. Dement. Geriatr. Cogn. Disord. 1998; 9(Suppl 1):6–12. [PubMed: 9716238]

Fazekas F, Kleinert R, Offenbacher H, Schmidt R, Kleinert G, Payer F, Radner H, Lechner H. Pathologic correlates of incidental MRI white matter signal hyperintensities. Neurology. 1993; 42:1683–1689. [PubMed: 8414012]

Friston KJ, Holmes AP, Worsley KJ, Poline JP, Frith CD, Frackowiak RSJ. Statistical parametric maps in functional imaging: A general linear approach. Human Brain Mapping. 1995; 2:189–210.

Gouw AA, Seewann A, Vrenken H, van der Flier WM, Rozemuller JM, Scheltens P, Geurts JJ. Heterogeneity of white matter hyperintensities in Alzheimer's disease: post-mortem quantitative MRI and neuropathology. Brain. 2008; 131:3286–3298. [PubMed: 18927145]

Head D, Buckner RL, Shimony JS, William LE, Akbudak E, Conturo TE, McAvoy M, Morris JC, Snyder AZ. Differential vulnerability of anterior white matter in nondemented aging with minimal acceleration in dementia of the Alzheimer type: evidence from diffusion tensor imaging. Cereb. Cortex. 2004; 14:410–423. [PubMed: 15028645]

Henry RG, Oh J, Nelson SJ, Pelletier D. Directional diffusion in relapsing-remitting multiple sclerosis: A possible in vivo signature of Wallerian degeneration. J. Magn. Reson. Imaging. 2003; 18:420–426. [PubMed: 14508778]

Huang H, Zhang J, Jiang H, Wakana S, Poetscher L, Miller MI, van Zijl PCM, Hillis AE, Wytik R, Mori S. DTI Tractography based Parcellation of White Matter: Application to the Mid-sagittal Morphology of Corpus Callosum. NeuroImage. 2005; 26:195–205. [PubMed: 15862219]

Huang J, Friedland RP, Auchus AP. Diffusion tensor imaging of normal-appearing white matter in mild cognitive impairment and early Alzheimer disease: preliminary evidence of axonal degeneration in the temporal lobe. AJNR Am. J. Neuroradiol. 2007; 28:1943–1948. [PubMed: 17905894]

Jack CR Jr, Petersen RC, Xu YC, O'Brien PC, Smith GE, Ivnik RJ, Tangalos EG, Kokmen E. Prediction of Alzheimer's disease with MRI-based hippocampal volume in mild cognitive impairment. Neurology. 1999; 52:1397–1403. [PubMed: 10227624]

Janke AL, de Zubicaray G, Rose SE, Griffin M, Chalk JB, Galloway GJ. 4D deformation modeling of cortical disease progression in Alzheimer's dementia. Magn. Reson. Med. 2001; 46:661–666. [PubMed: 11590641]

Jiang H, van Zijl PCM, Kim J, Pearlson GD, Mori S. DtiStudio: Resource program for diffusion tensor computation and fiber bundle tracking. Computer methods and programs in biomedicine. 2006; 81:106–116. [PubMed: 16413083]

Jones DK, Horsfield MA, Simmons A. Optimal strategies for measuring diffusion in anisotropic systems by magnetic resonance imaging. Magn Reson Med. 1999; 42:515–525. [PubMed: 10467296]

Mapstone M, Logan D, Duffy CJ. Cue integration for the perception and control of self-movement in ageing and Alzheimer's disease. Brain. 2006; 129:2931–2944. [PubMed: 17071922]

McKhann G, Drachman D, Folstein M, Katzman R, Price D, Stadlan EM. Clinical diagnosis of Alzheimer's disease: report of the NINCDS-ADRDA Work Group under the auspices of Department of Health and Human Services Task Force on Alzheimer's Disease. Neurology. 1984; 34:939–944. [PubMed: 6610841]

Medina D, Toledo-Morrell L, Urresta F, Gabrieli JD, Moseley M, Fleischman D, Bennett DA, Leurgans S, Turner DA, Stebbins GT. White matter changes in mild cognitive impairment and AD: a diffusion tensor imaging study. Neurobiol. Aging. 2006; 27:663–672. [PubMed: 16005548]

Mielke MM, Kozauer NA, Chan KCG, George M, Toroney J, Zerrate M, Bandeen-Roche K, Wang MC, van Zijl P, Pekar JJ, Mori S, Lyketsos CG, Albert M. Regionally-specific diffusion tensor imaging in mild cognitive impairment and Alzheimer's disease. Neuroimage. 2009; 46:47–53. [PubMed: 19457371]

Mori S, van Zijl PCM. Diffusion weighting by the trace of the diffusion tensor within a single scan. Magn. Reson. Med. 1995; 33:41–52. [PubMed: 7891534]

Mori S, Oishi K, Jiang H, Jiang L, Li X, Akhter K, Hua K, Faria AV, Mahmood A, Woods R, Toga AW, Pike GB, Neto PR, Evans A, Zhang J, Huang H, Miller MI, van Zijl PCM, Mazziotta J. Stereotaxic white matter atlas based on diffusion tensor imaging in an ICBM template. NeuroImage. 2008; 40:572–582.

Morris JC, Edland S, Clark C, Galasko D, Koss E, Mohs R, van Belle G, Fillenbaum G, Heyman A. The Consortium to Establish a Registry for Alzheimer's Disease (CERAD). Part I. Clinical and neuropsychological assessment of Alzheimer's disease. Neurology. 1989; 39:1159–1165. [PubMed: 2771064]

Moseley ME, Cohen Y, Kucharczyk J, Mintorovitch J, Asgari HS, Wendland MF, Tsuruda J, Norman D. Diffusion-weighted MR imaging of anisotropic water diffusion in cat central nervous system. Radiology. 1990; 176:439–445. [PubMed: 2367658]

Nestor PJ, Fryer TD, Smielewski P, Hodges JR. Limbic hypometabolism in Alzheimer's disease and mild cognitive impairment. Ann. Neurol. 2003; 54:343–351. [PubMed: 12953266]

Petersen RC, Smith GE, Waring SC, Ivnik RJ, Kokmen E, Tangelos EG. Aging, memory, and mild cognitive impairment. Int. Psychogeriatr. 1997; 9(Suppl. 1):65–69. [PubMed: 9447429]

Pievani M, Agosta F, Pagani E, Canu E, Sala S, Absinta M, Geroldi C, Ganzola R, Frisoni GB, Filippi M. Hum. Brain Mapp. 2010 (in press).

Pierpaoli C, Jezzard P, Basser PJ, Barnett A, Di Chiro G. Diffusion tensor MR imaging of human brain. Radiology. 1996; 201:637–648. [PubMed: 8939209]

Pierpaoli C, Barnett A, Pajevic S, Chen R, Penix LR, Virta A, Basser P. Water diffusion changes in Wallerian degeneration and their dependence on white matter architecture. Neuroimage. 2001; 13:1174–1185. [PubMed: 11352623]

Pinheiro, JC.; Bates, DM. Mixed-Effects Models in S and S-Plus. Springer; 2000.

Pounds S, Morris SW. Estimating the occurrence of false positives and false negatives in microarray studies by approximating and partitioning the empirical distribution of p-values. Bioinformatics. 2003; 19:1236–1242. [PubMed: 12835267]

Raoux N, Amieva H, Le Goff M, Auriacombe S, Carcaillon L, Letenneur L, Dartigues JF. Clustering and switching processes in semantic verbal fluency in the course of Alzheimer's disease subjects: results from the PAQUID longitudinal study. Cortex. 2008; 44:1188–1196. [PubMed: 18761132]

Roher AE, Weiss N, Kokjohn TA, Kuo YM, Kalback W, Anthony J, Watson D, Luehrs DC, Sue L, Walker D, Emmerling M, Goux W, Beach T. Increased Aβ peptides and reduced cholesterol and myelin proteins characterize white matter degeneration in Alzheimer's disease. Biochemistry. 2002; 41:11080–11090. [PubMed: 12220172]

Román GC, Tatemichi TK, Erkinjuntti T, Cummings JL, Masdeu JC, Garcia JH, Amaducci L, Orgogozo JM, Brun A, Hofman A, Moody DM, O'Brien MD, Yamaguchi T, Grafman J, Drayer BP, Bennett DA, Fisher M, Ogata J, Kokmen E, Bermejo F, Wolf PA, Gorelick PB, Bick KL, Pajeau AK, Bell MA, DeCarli C, Culebras A, Korczyn AD, Bogousslavsky J, Hartmann A, Scheinberg P. Vascular dementia: diagnostic criteria for research studies. Report of NINDS-AIREN International Workshop. Neurology. 1993; 43:250–260. [PubMed: 8094895]

Roosendaal SD, Geurts JJ, Vrenken H, Hulst HE, Cover KS, Castelijns JA, Pouwels PJ, Barkhof F. Regional DTI differences in multiple sclerosis patients. Neuroimage. 2009; 44:1397–1403. [PubMed: 19027076]

Rose SE, Chen F, Chalk JB, Zelaya FO, Strugnell WE, Benson M, Semple J, Doddrell DM. Loss of connectivity in Alzheimer's disease: an evaluation of white matter tract integrity with colour coded MR diffusion tensor imaging. J. Neurol. Neurosurg. Psychiatry. 2000; 69:528–530. [PubMed: 10990518]

Scheltens P, Barkhof F, Leys D, Wolters EC, Ravid R, Kamphorst W. Histopathologic correlates of white matter changes on MRI in Alzheimer's disease and normal aging. Neurology. 1995; 45:883–888. [PubMed: 7746401]

Seeley WW, Crawford RK, Zhou J, Miller BL, Greicius MD. Neurodegenerative diseases target large-scale human brainnetworks. Neuron. 2009; 62:42–52. [PubMed: 19376066]

Schmahmann, JD.; Pandya, DN. Fiber pathways of the brain. Oxford University Press; 2006.

Shen D, Davatzikos C. HAMMER: Hierachical attribute matching mechanism for elastic registration. IEEE Trans. on Medical Imaging. 2002; 21:1421–1439.

Smith CD, Snowdon DA, Wang H, Markesbery WR. White matter volumes and periventricular white matter hyperintensities in aging and dementia. Neurology. 2000; 54:838–842. [PubMed: 10690973]

Smith CD, Chebrolu H, Andersen AH, Powell DA, Lovell MA, Xiong S, Gold BT. White matter diffusion alterations in normal women at risk of Alzheimer's disease. Neurobiology of Aging. 2008 In Press.

Smith SM, Jenkinson M, Johansen-Berg H, Rueckert D, Nichols TE, Mackay CE, Watkins KE, Ciccarelli O, Cader MZ, Matthews PM, Behrens TEJ. Tract-based spatial statistics: Voxelwise analysis of multi-subject diffusion data. NeuroImage. 2006; 31:1487–1505. [PubMed: 16624579]

Song SK, Sun SW, Ramsbottom MJ, Chang C, Russell J, Cross AH. Dysmyelination revealed through MRI as increased radial (but unchanged axial) diffusion of water. Neuroimage. 2002; 17:1429–1436. [PubMed: 12414282]

Song SK, Sun SW, Ju WK, Lin SJ, Cross AH, Neurfeld AH. Diffusion tensor imaging detects and differentiates axon and myelin degenerationin mouse optic nerve after retinal ischemia. Neuroimage. 2003; 20:1714–1722. [PubMed: 14642481]

Stahl R, Dietrich O, Teipel SJ, Hampel H, Reiser MF, Schoenberg SO. White matter damage in Alzheimer disease and mild cognitive impairment: assessment with diffusion-tensor MR imaging and parallel imaging techniques. Radiology. 2007; 24:483–492. [PubMed: 17456872]

Stoub TR, deToledo-Morrell L, Stebbins GT, Leurgans S, Bennett DA, Shah RC. Hippocampal disconnection contributes to memory dysfunction in individuals at risk for Alzheimer's disease. Proc. Natl. Acad. Sci. USA. 2006; 103:10041–10045. [PubMed: 16785436]

Stricker NH, Schweinsburg BC, Delano-Wood L, Wierenga CE, Bangen KJ, Haaland KY, Frank LR, Salmon DP, Bondi MW. Decreased white matter integrity in late-myelinating fiber pathways in Alzheimer's disease supports retrogenesis. NeuroImage. 2009; 45:10–16. [PubMed: 19100839]

Takahashi S, Yonezawa H, Takahashi J, Kudo M, Inoue T, Tohgi H. Selective reduction of diffusion anisotropy in white matter of Alzheimer disease brains measured by 3.0 Tesla magnetic resonance imaging. Neuroscience Letters. 2002; 332:45–48. [PubMed: 12377381]

Thompson PM, Mega RS, Woods RP, Zoumalan CI, Lindshield CJ, Blanton RE, Moussai J, Holmes CJ, Cummings JL, Toga AW. Cortical change in Alzheimer's disease detected with a disease-specific population-based brain atlas. Cereb. Cortex. 2001; 11:1–16. [PubMed: 11113031]

Thompson PM, Hayashi KM, de Zubicaray G, Janke AL, Rose SE, Semple J, Herman D, Hong MS, Dittmer SS, Doddrell DM, Toga AW. Dynamics of gray matter loss in Alzheimer's disease. J. Neurosci. 2003; 23:993–1005.

Villain N, Desgranges B, Viader F, Sayette, de la V, Mezenge F, Landeau B, Baron J-C, Eustache F, Chetelat G. Relationships between Hippocampal atrophy, white matter disruption, and gray matter hypometabolism in Alzheimer's disease. J. Neurosci. 2008; 28:6174–6181. [PubMed: 18550759]

Wakana S, Caprihan A, Panzenboeck MM, Fallon JH, Perry M, Gollub RL, Hua K, Zhang J, Jiang H, Dubey P, Blitz A, van Zijl P, Mori S. Reproducibility of quantitative tractography methods applied to cerebral white matter. Neuroimage. 2007; 36:630–644. [PubMed: 17481925]

Weiner MW. Expanding ventricles may detect preclinical Alzheimer disease. Neurology. 2008; 70:824–825. [PubMed: 18332339]

Wheeler-Kingshott CAM, Cercignani M. About "axial" and "radial" diffusivities. Magn. Reson. Med. 2009; 61:1255–1260. [PubMed: 19253405]

Woods RP, Grafton ST, Holmes CJ, Cherry SR, Mazziotta JC. Automated image registration: I. General methods and intrasubject, intramodality validation. J. Comput. Assist. Tomogr. 1998; 22:139–152. [PubMed: 9448779]

Xie S, Xiao JX, Gong GL, Zang YF, Wang YH, Wu HK, Jiang XX. Voxel-based detection of white matter abnormalities in mild Alzheimer disease. Neurology. 2006; 66:1845–1849. [PubMed: 16801648]

Yap PT, Wu G, Zhu H, Lin W, Shen D. TIMER: Tensor Image Morphing for Elastic Registration. Neuroimage. 2009; 47:549–563. [PubMed: 19398022]

Zhang H, Avants BB, Yushkevich PA, Woo JH, Wang S, McCluskey LF, Elman LB, Melhem ER, Gee JC. High-dimensional spatial normalization of diffusion tensor images improves the detection

of white matter differences: an example study using amyotrophic lateral sclerosis. IEEE Trans. Med. Imag. 2007; 26:1585–1597.

Zhang Y, Schuff N, Jahng GH, Bayne W, Mori S, Schad L, Mueller S, Du AT, Kramer JH, Yaffe K, Chui H, Jagust WJ, Miller BL, Weiner MW. Diffusion tensor imaging of cingulum fibers in mild cognitive impairment and Alzheimer disease. Neurology. 2007; 68:13–19. [PubMed: 17200485]

Zhuang L, Wen W, Zhu W, Trollor J, Kochan N, Crawford J, Reppermund S, Brodaty H, Sachdev P. White matter integrity in mild cognitive impairment: A tract-based spatial statistics study. Neuroimage. 2010 (in press).

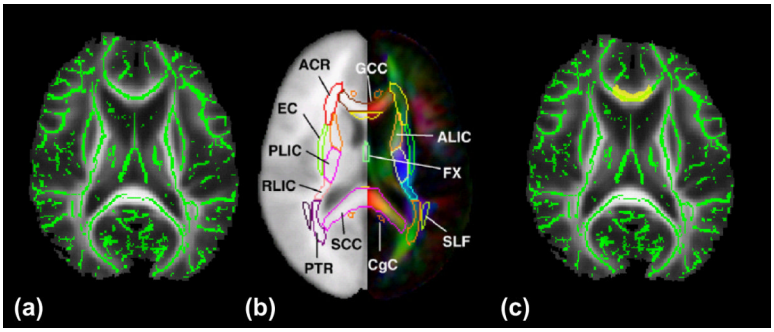

Figure 1.

Projection of FA value to the core white matter. Green skeleton is overlaid on the averaged FA map; (b) the ICBM-DTI-81 digital white matter atlas; (c) as an example, the genu of corpus callosum (GCC) (yellow shadow) is transferred from the digital atlas to cover the green skeleton overlaid on the averaged FA map. Abbreviations of the white matter tract names can be found in the legend of Fig. 2.

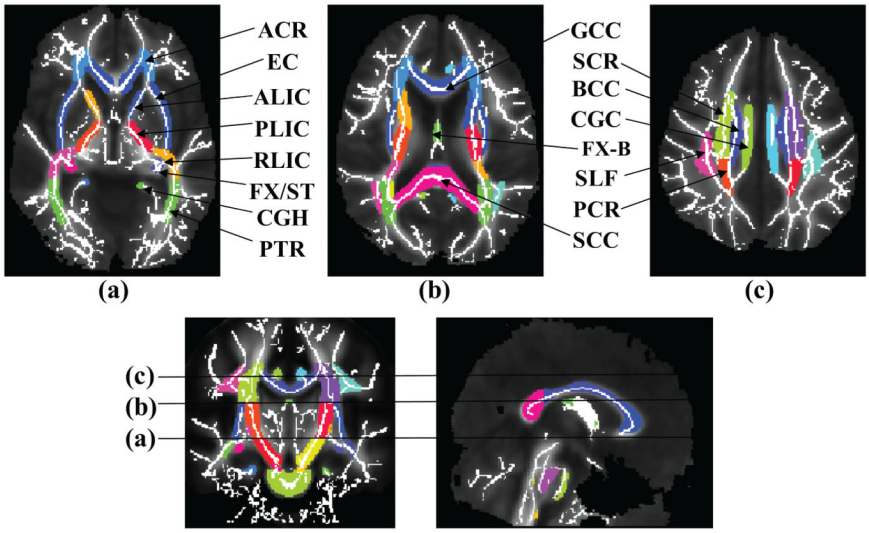

Figure 2.

Mean FA (gray scale) and skeleton of all subjects overlaid by the atlas labels in the ICBM-DTI-81 space. Colored regions indicate major white matter tracts. The skeleton from averaged FA maps is shown as white solid curve. L and R indicate left and right. Abbreviations of white matter tracts are as follows. ACR: Anterior corona radiata; ALIC: Anterior limb of internal capsule; BCC: Body of corpus callosum; CGC: Cingulum bundle at cingulate gyrus; CGH: Cingulum bundle in hippocampus; CST: Corticospinal tract; EC: External capsule; FX: Fornix; FX-B: Body of fornix; GCC: Genu of corpus callosum; IFO: Inferior fronto-occipital fasciculus left; ILF: Inferior longitudinal fasciculus; PCR: Posterior corona radiate; PLIC: Posterior limb of internal capsule; PTR: Posterior thalamic radiation; RLIC: Retrolenticular part of internal capsule; SCC: Splenium of corpus callosum; SCR: Superior corona radiate; SLF: Superior longitudinal fasciculus; ST: Stria terminalis; UNC: Uncinate fasciculus.

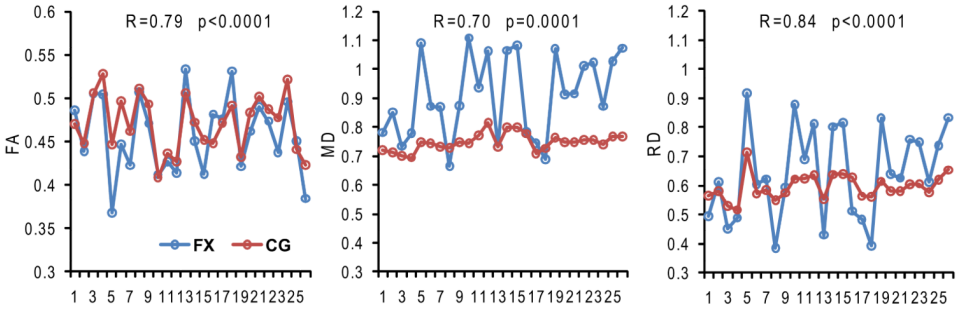

Figure 3.

Synchronized changes of FA, MD and RD from left to right of fornix (FX, blue) and cingulum bundle (CG, red), both of which are part of limbic tract group. Each point represents data from an AD patient. The horizontal axis indicates index of different AD patients. Correlation coefficient (R) and p value of correlation are also displayed in each panel.

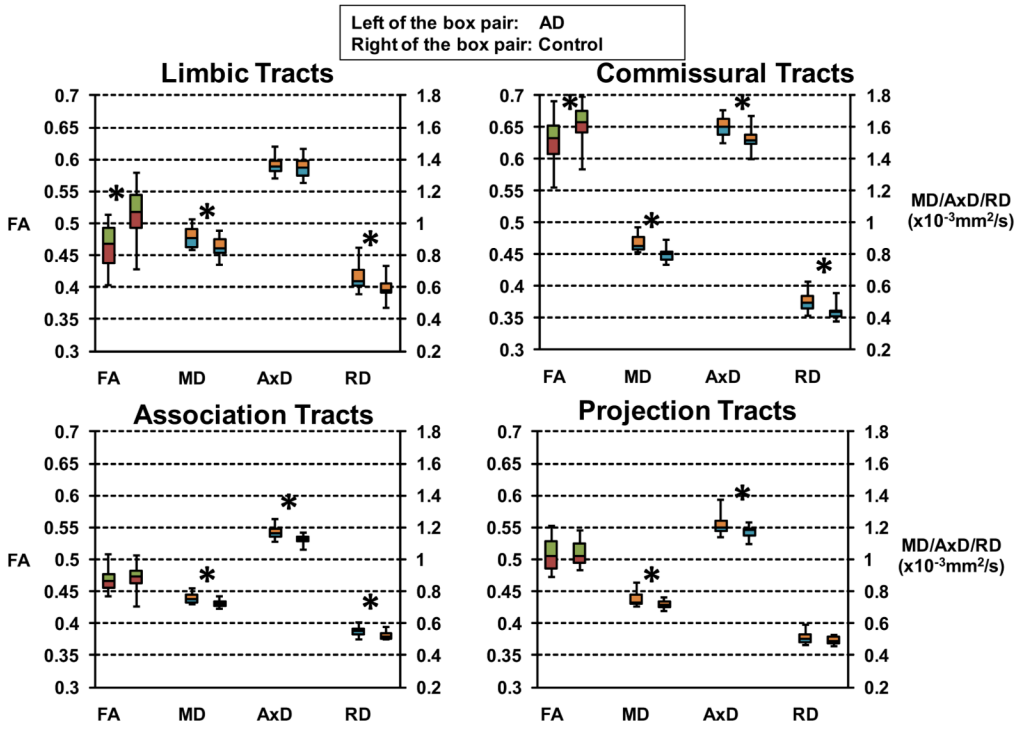

Figure 4.

Boxplots of FA, MD, AxD and RD of limbic, commissural, association and projection tract groups for AD patients (left of the box pair) compared with the controls (right of the box pair). Statistically significant differences after FDR correction are marked with asterisks.

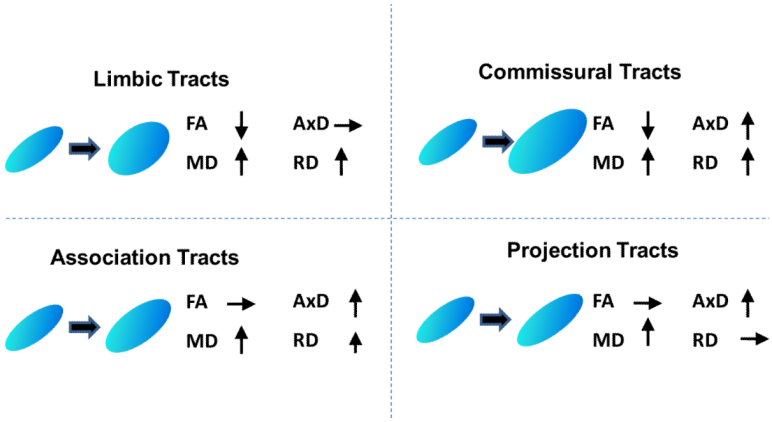

Figure 5.
Tensor change profiles of limbic, commissural, association and projection tract groups reflected by full tensor characterization of FA, MD, AxD and RD, the four metrics derived from diffusion tensor.

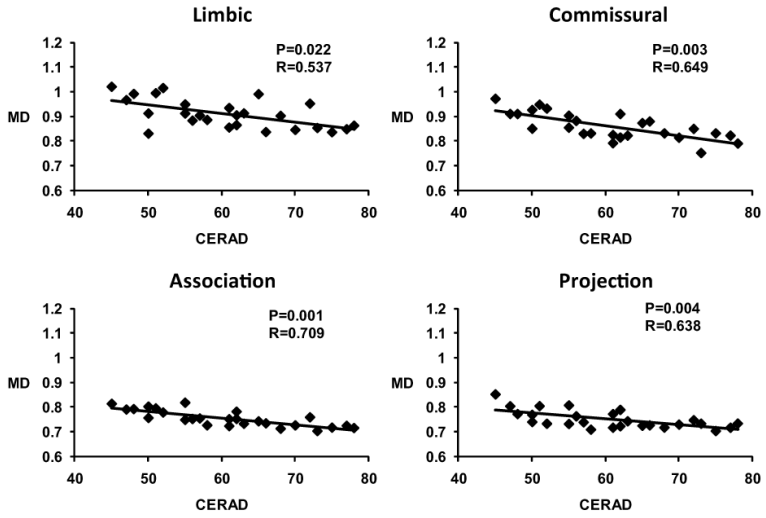

Figure 6.

Statistically significant correlations (after age and education correction) between MD and CERAD total scores of AD patients for all limbic, commissural, association and projection tract groups.

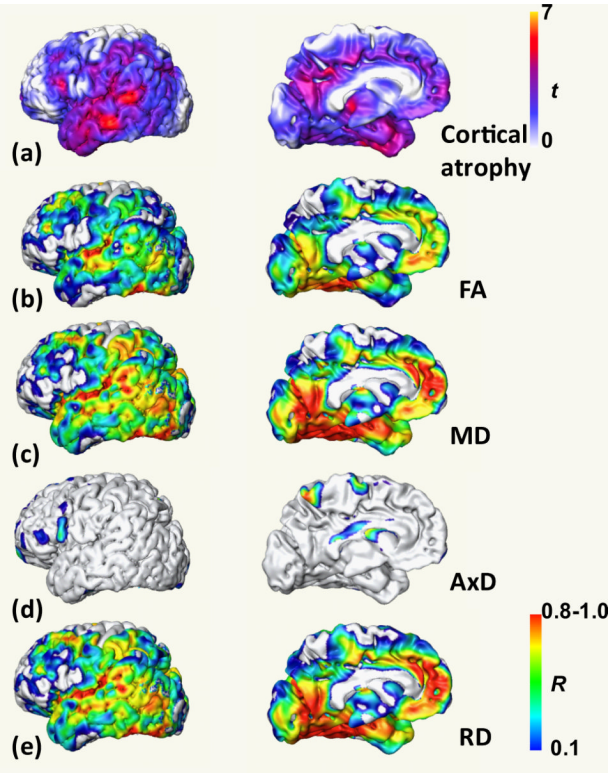

Figure 7.
Cortical atrophy t value map (a) is displayed in the top panel. Correlation coefficient maps for correlation of FA (b), MD (c), AxD (d) and RD (e) of limbic tract group with cortical atrophy are displayed in the lower panels. The top and bottom color bars indicate t value of cortical atrophy and correlation coefficient, respectively.

Table 1

Demographic and clinical features of AD patients and healthy controls.

	AD patients	MCI	Controls	P
Number	26	11	24	---
Age (years, mean±SD)	70.8±8.2	69.1±7.3	69.5±7.1	0.54
Gender, female	11 (42.3%)	6 (54.5%)	14 (58.3%)	0.21
Education (years, mean±SD)	15.3±3.3	15.2±1.9	15.1±3.8	0.61
Hachinski score (mean±SD)	0.7±0.6	0.6±0.9	0.5±0.7	0.25
MMSE (mean±SD)	23.2±2.5	27.3±2.1	29.4±0.8	<0.001
CERAD (mean±SD)	60.8±9.6	77.1±9.7	84.5±7.2	<0.001

Table 2

Mean values of FA, MD, AxD and RD of major limbic tracts of AD patients and controls, standard deviation of these metrics of AD patients, t and p values ($p^{\dagger}$) from tract level comparison and p ($p^{\ddagger}$) value from tract group level comparison between AD and control are listed. Double asterisks and bold indicate statistically significant differences after FDR correction. The abbreviations for tables can be found in legend of Fig. 2.

		Limbic Tracts						
		FX-ST/L	***FX-ST/R***	***FX-B***	***CGC-L***	***CGC-R***	***CGH-L***	***CGH-R***
FA	AD	0.52	0.48	0.41	0.50	0.45	0.50	0.47
	Diff (AD-Ctr)	−0.052	−0.049	−0.085	−0.051	−0.040	−0.050	−0.039
	Std. Error	0.014	0.013	0.031	0.016	0.012	0.018	0.016
	T	−3.77	−3.60	−2.73	−3.21	−3.43	−2.84	−2.51
	$p^{\dagger}$	**<0.001****	**0.001****	**0.01****	**0.003****	**0.002****	**0.008****	**0.02****
	Tract group $p^{\ddagger}$	**<0.001****						
MD ($10^{-3}mm^2/S$)	AD	0.79	0.80	0.97	0.76	0.79	0.70	0.69
	Diff (AD-Ctr)	0.044	0.025	0.15	0.027	0.045	0.043	0.011
	Std. Error	0.014	0.023	0.061	0.011	0.021	0.017	0.013
	T	3.17	1.12	2.55	2.59	2.10	2.58	0.86
	$p^{\dagger}$	**0.003****	0.27	**0.02****	**0.01****	**0.04****	**0.01****	0.4
	Tract group $p^{\ddagger}$	**0.007****						
AxD ($10^{-3}mm^2/S$)	AD	1.26	1.23	1.60	1.24	1.20	1.12	1.06
	Diff (AD-Ctr)	−0.012	−0.036	−0.081	−0.019	0.021	−0.019	−0.035
	Std. Error	0.011	0.026	0.051	0.021	0.016	0.013	0.023
	T	−0.52	−1.37	−1.24	−0.78	0.73	−0.64	−1.48
	$p^{\dagger}$	0.61	0.18	0.22	0.44	0.47	0.52	0.15
	Tract group $p^{\ddagger}$	0.19						
RD ($10^{-3}mm^2/S$)	AD	0.54	0.58	0.66	0.53	0.58	0.50	0.51
	Diff (AD-Ctr)	0.071	0.052	0.057	0.056	0.062	0.071	0.040
	Std. Error	0.017	0.023	0.021	0.015	0.021	0.023	0.015
	T	4.24	2.24	2.65	3.64	2.90	3.09	2.74

Limbic Tracts								
		FX-ST/L	***FX-ST/R***	***FX-B***	***CGC-L***	***CGC-R***	***CGH-L***	***CGH-R***
	$p^{\dagger}$	**<0.001****	**0.03****	**0.01****	**<0.001****	**0.007****	**0.004****	**0.01****
	Tract group $p^{\ddagger}$	**0.002****						

Table 3

Mean values of FA, MD, AxD and RD of major commissural tracts of AD patients and controls, standard deviation of these metrics of AD patients, t and p values ($p^{\dagger}$) from tract level comparison and p ($p^{\ddagger}$) value from tract group level comparison between AD and control are listed. Double asterisks and bold indicate statistically significant differences after FDR correction. The abbreviations for tables can be found in legend of Fig. 2.

Commissural Tracts				
		GCC	***BCC***	***SCC***
FA	AD	0.63	0.57	0.70
	Diff (AD-Ctr)	−0.011	−0.049	−0.012
	Std. Error	0.005	0.011	0.008
	T	−1.16	−3.73	−0.75
	$p^{\dagger}$	0.25	**<0.001****	0.45
	Tract group $p^{\ddagger}$	**0.011****		
MD ($10^{-3}mm^2/S$)	AD	0.87	0.92	0.81
	Diff (AD-Ctr)	0.062	0.083	0.065
	Std. Error	0.016	0.017	0.016
	T	3.98	4.84	4.15
	$p^{\dagger}$	**<0.001****	**<0.001****	**<0.001****
	Tract group $p^{\ddagger}$	**<0.001****		
AxD ($10^{-3}mm^2/S$)	AD	1.60	1.60	1.62
	Diff (AD-Ctr)	0.091	0.051	0.112
	Std. Error	0.023	0.021	0.013
	T	3.84	2.11	3.71
	$p^{\dagger}$	**<0.001****	**0.042****	**<0.001****
	Tract group $p^{\ddagger}$	**0.004****		
RD ($10^{-3}mm^2/S$)	AD	0.50	0.58	0.42
	Diff (AD-Ctr)	0.046	0.096	0.045
	Std. Error	0.015	0.025	0.016
	T	3.16	4.74	2.82
	$p^{\dagger}$	**0.003****	**<0.001****	**0.008****
	Tract group $p^{\ddagger}$	**0.001****		

Table 4

Mean values of FA, MD, AxD and RD of major association tracts of AD patients and controls, standard deviation of these metrics of AD patients, t and p values ($p^{\dagger}$) from tract level comparison and p ($p^{\ddagger}$) value from tract group level comparison between AD and control are listed. Double asterisks and bold indicate statistically significant differences after FDR correction. The abbreviations for tables can be found in legend of Fig. 2.

		Association Tracts					
		SLF-L	***SLF-R***	***SFO-L***	***SFO-R***	***EC-L***	***EC-R***
FA	AD	0.50	0.52	0.56	0.43	0.43	0.56
	Diff (AD-Ctr)	−0.004	−0.005	0.015	−0.013	0.002	0.015
	Std. Error	0.004	0.004	0.012	0.009	0.001	0.012
	t	−0.55	−0.31	0.94	−1.51	0.19	0.94
	$p^{\dagger}$	0.59	0.76	0.35	0.14	0.85	0.35
	Tract group $p^{\ddagger}$	0.28					
MD ($10^{-3}mm^2/S$)	AD	0.74	0.75	0.70	0.71	0.78	0.77
	Diff (AD-Ctr)	0.033	0.024	0.039	0.024	0.054	0.035
	Std. Error	0.011	0.009	0.017	0.013	0.013	0.013
	T	3.07	2.69	2.32	1.91	4.10	2.71
	$p^{\dagger}$	**0.004****	**0.011****	**0.027****	0.065	**0.002****	**0.010****
	Tract group $p^{\ddagger}$	**0.003****					
AxD ($10^{-3}mm^2/S$)	AD	1.18	1.18	1.15	1.22	1.16	1.14
	Diff (AD-Ctr)	0.051	0.053	0.061	0.063	0.062	0.045
	Std. Error	0.016	0.014	0.030	0.031	0.020	0.016
	t	3.13	4.61	2.05	2.05	3.12	2.91
	$p^{\dagger}$	**0.004****	**<0.001****	**0.049****	**0.048****	**0.004****	**0.006****
	Tract group $p^{\ddagger}$	**0.002****					
RD ($10^{-3}mm^2/S$)	AD	0.51	0.53	0.47	0.45	0.59	0.59
	Diff (AD-Ctr)	0.024	0.011	0.027	0.027	0.051	0.031
	Std. Error	0.011	0.01	0.017	0.012	0.012	0.013
	t	2.26	1.01	1.62	0.22	4.26	2.42

Association Tracts							
		SLF-L	***SLF-R***	***SFO-L***	***SFO-R***	***EC-L***	***EC-R***
	$p^{\dagger}$	**0.03****	0.32	0.11	0.83	**<0.001****	**0.021****
	Tract group $p^{\ddagger}$	**0.006****					

Table 5

Mean values of FA, MD, AxD and RD of major projection tracts of AD patients and controls, standard deviation of these metrics of AD patients, t and p values ($p^{\dagger}$) from tract level comparison and p ($p^{\ddagger}$) value from tract group level comparison between AD and control are listed. Double asterisks and bold indicate statistically significant differences after FDR correction. The abbreviations for tables can be found in legend of Fig. 2.

		Projection Tracts									
		ACR-L	***ACR-R***	***PCR-L***	***PCR-R***	***SCR-L***	***SCR-R***	***ALIC-L***	***ALIC-R***	***PLIC-L***	***PLIC-R***
FA	AD	0.42	0.40	0.50	0.48	0.48	0.46	0.56	0.58	0.69	0.72
	Diff (AD-Ctr)	−0.011	−0.028	0.009	0.007	0.006	0.002	0.003	0.007	0.008	0.022
	Std. Error	0.010	0.011	0.008	0.005	0.005	0.002	0.002	0.006	0.005	0.014
	t	−1.01	−2.63	0.83	0.58	0.56	0.22	0.34	0.60	0.71	1.54
	$p^{\dagger}$	0.32	**0.013****	0.41	0.57	0.58	0.82	0.73	0.55	0.48	0.13
	Tract group $p^{\ddagger}$	0.50									
MD ($10^{-3}mm^2/S$)	AD	0.79	0.80	0.78	0.78	0.75	0.75	0.73	0.73	0.68	0.65
	Diff (AD-Ctr)	0.043	0.051	0.37	0.033	0.042	0.030	0.026	0.014	0.009	−0.014
	Std. Error	0.016	0.016	0.019	0.016	0.015	0.013	0.012	0.011	0.008	0.011
	T	2.73	3.14	1.96	2.09	2.80	2.41	2.27	0.96	1.07	−1.09
	$p^{\dagger}$	**0.010****	**0.003****	0.058	**0.043****	**0.008****	**0.022****	**0.029****	0.34	0.30	0.28
	Tract group $p^{\ddagger}$	**0.017****									
AxD ($10^{-3}mm^2/S$)	AD	1.18	1.17	1.25	1.22	1.19	1.17	1.25	1.27	1.34	1.31
	Diff (AD-Ctr)	0.054	0.041	0.068	0.059	0.078	0.054	0.051	0.032	0.031	0.002
	Std. Error	0.017	0.018	0.027	0.018	0.027	0.021	0.018	0.016	0.011	0.001
	T	3.15	2.22	2.49	3.27	2.95	2.61	2.81	1.34	1.38	0.09
	$p^{\dagger}$	**0.003****	**0.033****	**0.018****	**0.003****	**0.006****	**0.013****	**0.008****	0.19	0.18	0.93
	Tract group $p^{\ddagger}$	**0.017****									
RD ($10^{-3}mm^2/S$)	AD	0.60	0.61	0.54	0.55	0.53	0.54	0.47	0.46	0.35	0.33
	Diff (AD-Ctr)	0.038	0.056	0.023	0.019	0.027	0.018	0.013	0.057	−0.001	−0.019
	Std. Error	0.016	0.017	0.011	0.011	0.017	0.012	0.011	0.013	0.001	0.014
	T	2.33	3.28	1.25	1.10	1.92	1.52	1.09	0.43	−0.11	−1.33
	$p^{\dagger}$	**0.025****	**0.002****	0.22	0.28	0.064	0.14	0.28	0.67	0.91	0.19
	Tract group $p^{\ddagger}$	0.062									

Table 6

Mean values of FA, MD, AxD and RD of limbic, commissural, association and projection tract groups of aMCI subjects, difference of these measurements between aMCI and control and p values ($p^{\ddagger}$) from tract group comparison between aMCI and control are listed. Double asterisks and bold indicate statistically significant differences after FDR correction.

		Limbic	Commissural	Association	Projection
FA	aMCI	0.48	0.65	0.46	0.50
	Diff (aMCI-Ctr)	−0.041	−0.02	−0.025	−0.028
	Tract group $p^{\ddagger}$	**0.041****	0.19	0.082	0.31
MD	aMCI	0.84	0.81	0.72	0.72
	Diff (aMCI-Ctr)	0.039	0.032	0.016	0.014
	Tract group $p^{\ddagger}$	**0.032****	**0.046****	0.071	0.051
AxD	aMCI	1.28	1.50	1.09	1.15
	Diff (aMCI-Ctr)	0.002	0.021	0.009	0.016
	Tract group $p^{\ddagger}$	0.67	0.11	0.56	0.20
RD	aMCI	0.59	0.42	0.51	0.48
	Diff (aMCI-Ctr)	0.049	0.017	0.018	0.013
	Tract group $p^{\ddagger}$	**0.029****	0.15	0.051	0.11